Dark Matter Dilution Mechanism through the Lens of Large-Scale Structure

Miha Nemevšek[1,2,*] and Yue Zhang[3,†]
[1]Jožef Stefan Institute, Jamova 39, 1000 Ljubljana, Slovenia
[2]Faculty of Mathematics and Physics, University of Ljubljana, Jadranska 19, 1000 Ljubljana, Slovenia
[3]Department of Physics, Carleton University, Ottawa, Ontario K1S 5B6, Canada

(Received 30 June 2022; accepted 1 March 2023; published 23 March 2023)

Entropy production is a necessary ingredient for addressing the overpopulation of thermal relics. It is widely employed in particle physics models for explaining the origin of dark matter. A long-lived particle that decays to the known particles, while dominating the universe, plays the role of the dilutor. We point out the impact of its partial decay to dark matter on the primordial matter power spectrum. For the first time, we derive a stringent limit on the branching ratio of the dilutor to dark matter from large scale structure observation using the sloan digital sky survey data. This offers a novel tool for testing models with a dark matter dilution mechanism. We apply it to the left-right symmetric model and show that it firmly excludes a large portion of parameter space for right-handed neutrino warm dark matter.

DOI: 10.1103/PhysRevLett.130.121002

Introduction.—The nature of dark matter (DM) is a tantalizing puzzle about our universe and new elementary particle(s) are arguably the most compelling DM candidates. Their nongravitational interactions may establish thermal contact with the known particles in the early universe and dynamically produce the observed DM relic density.

The famous example of this kind is the weakly-interacting massive particle "WIMP miracle," where the DM mass is pinned around the electroweak scale by the freeze-out mechanism [1]. Going to smaller masses sometimes requires the existence of a new light dark force carrier, leading to the "dark-sector" theories [2]. Alternatively, if the mediator remains heavy, a light DM particle would freeze-out relativistically. If nothing else happens, such relic will either overclose the universe or remain too hot for structure formation. Moreover, excessive DM production could take place via feeble processes [3,4]. An attractive mechanism for addressing such overabundance problems resorts to late time entropy production, injected by the decay of a long-lived particle [5–21], often referred to as the "dilutor." Such a dilution mechanism has been utilized in a wide variety of theory contexts, e.g., sterile neutrino DM from gauge extensions [9,10,18], gravitino DM via freeze in or out production [6,7,21], and glueball DM [14].

In this Letter, we point out and investigate an important aspect of generic DM dilution mechanisms—the (subdominant) decay of the dilutor into DM. Such channels hamper the goal of diluting the DM relic density and are often omitted in simplified analyses. However, they do arise in well-motivated ultraviolet complete theories, either at tree level or via radiative corrections, with its branching ratio fixed by the theory structure. This ratio serves as a key parameter that characterizes the dilution mechanism.

Our main result is to show that DM produced by the dilutor decay is typically energetic and can have a profound impact on the primordial matter power spectrum. We show that the existing large scale structure (LSS) data already constrain the branching ratio of this decay mode to percent level. This is a general result and serves as a goalpost for various DM dilution mechanisms. A concrete example of right-handed neutrino DM from the minimal left-right symmetric model (LRSM) [22–24], will be discussed.

Entropy dilution for relic density.—Hereafter, we refer to the DM as X and the dilutor as Y. Both are in thermal equilibrium with the visible sector at early times and decouple relativistically at similar temperatures. This makes their initial abundances equal, barring spin factors. The correct DM relic density is obtained if the dilutor Y is sufficiently long-lived, becomes nonrelativistic, and

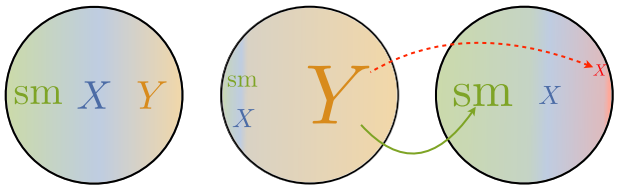

FIG. 1. Schematic illustration of the DM dilution mechanism: relativistic freeze-out, dilutor matter domination, entropy injection (dashed red line), and DM repopulation (solid green line).

dominates the energy density before decaying away, as shown in Fig. 1.

The dilutor Y reheats the universe by decaying into the visible final states "SM," however, it can also decay into X,

$$Y \to \mathrm{SM}, \qquad Y \to nX(+m\mathrm{SM}), \tag{1}$$

where $n, m \in \mathbb{Z}^+$ count the multiplicity of X and SM particles, respectively. The first decay channel dumps entropy into the visible sector and dilutes the primordial thermal population of X. The second channel, whose branching ratio is given by Br_X, produces a secondary nonthermal population of X that repopulates DM and contributes to its final relic density. The bracket in (1) includes the possibility that the secondary channel is completely dark, without any "SM" in the final state. In the absence of extended dark sectors, the branching ratio of the first channel is $1 - \mathrm{Br}_X$.

After dilution, DM becomes nonrelativistic with the relic abundance [9,10]

$$\Omega_X \simeq 0.26(1 + n\mathrm{Br}_X)\left(\frac{m_X}{1\ \mathrm{keV}}\right)\left(\frac{1\ \mathrm{GeV}}{m_Y}\right)\sqrt{\frac{1\ \mathrm{sec}}{\tau_Y}}, \tag{2}$$

derived under the sudden decay approximation [5]. See the supplemental material [25] for more details. Using $H(T_{\mathrm{RH}})\tau_Y = 1$, Y reheats the universe to a temperature

$$T_{\mathrm{RH}} \simeq \frac{1\ \mathrm{MeV}}{g_*(T_{\mathrm{RH}})^{1/4}}\left(\frac{m_Y}{10^6 m_X}\right), \tag{3}$$

where the lifetime of Y is determined by m_Y/m_X from (2). For successful big-bang nucleosynthesis (BBN), we need $T_{\mathrm{RH}} > \mathrm{MeV}$, which requires a large hierarchy between the dilutor and DM masses $m_Y \gg m_X$.

Such scenarios feature two distinct populations of X: the primordial and the secondary one. The thermal primordial component gets cooled by entropy production from Y decays below the photon temperature. Conversely, the secondary X's are more energetic and carry the energy on the order of $m_Y/(n+m) \gg T_X$, where T_X is the temperature of the primordial X. We assume that X remains collisionless after Y decay.

Consider the phase space distribution of X particles, $f_X(x,t)$, which is a function of time t and $x = E_X/T_X$. With this convention, the $f_X(x,t)$ satisfies

$$\frac{T_X^3}{2\pi^2}x^2\dot{f}_X(x,t) = \frac{\rho_Y(t)\Gamma_Y \mathrm{Br}_X}{m_Y}\frac{T_X}{m_Y}g(\omega), \tag{4}$$

where $\omega = E_X/m_Y$. The $g(\omega)$ function is the distribution of the energy fraction carried by X in the rest frame of Y. Its form is model dependent and normalized to $\int d\omega g(\omega) = n$. Averaging the energy over $g(\omega)$ gives

TABLE I. The energy fraction distribution $g(\omega)$, taken away by X in the rest frame of Y, and its integrals $n = \int g$, $y = \int \omega g$. The first row applies to the LRSM, where a single X ($n = 1$) is produced via a three-body decay. The second corresponds to a long-lived scalar, where $\Phi \to XX$ produces two DM states ($n = 2$), with δ being the Dirac delta function.

	n	$g(\omega)$	$\omega_{\max}$	y
LRSM	1	$16\omega^2(3-4\omega)$	1/2	7/20
Long-lived scalar	2	$2\delta(\omega - 1/2)$	⋯	1

$$y = \int d\omega\, \omega g(\omega), \tag{5}$$

which characterizes the energy fraction carried by X in the $Y \to nX(+m\mathrm{SM})$ decay.

For concreteness we consider the two models:

(1) the LRSM, where X is the lightest right-handed neutrino N_1 and Y is a heavier N_2, which undergoes a three-body decay into N_1 plus two charged leptons, mediated by the W_R gauge boson [9,10,18];

(2) a long-lived scalar Φ with a partial decay width into two fermionic DM. Φ may be incarnated as a modulus field in supersymmetric theories [6,26].

The corresponding g functions and n, y integrals are summarized in Table I. The masses of final-state charged leptons are neglected here.

The time dependence in the energy density ρ_Y can be computed by solving the coupled Boltzmann equations

$$\dot{\rho}_Y + 3H\rho_Y = -\Gamma_Y\rho_Y, \tag{6}$$

$$\dot{\rho}_X + 4H\rho_X = y\mathrm{Br}_X\Gamma_Y\rho_Y, \tag{7}$$

$$\dot{\rho}_{\mathrm{SM}} + 4H\rho_{\mathrm{SM}} \simeq (1 - y\mathrm{Br}_X)\Gamma_Y\rho_Y, \tag{8}$$

where ρ_{SM} is the energy density carried by relativistic visible particles and $H^2 = 8\pi G_N(\rho_Y + \rho_X + \rho_{\mathrm{SM}})/3$ is the Hubble parameter. This set of equations applies for nonrelativistic Y, while the X population remains ultrarelativistic. We neglect the temperature dependence of g_* in Eq. (8). Defining $\zeta = \ln a$ to keep track of time, the f_X can be solved as

$$f_X(x) = \frac{1}{e^x + 1} + \frac{2\pi^2}{x^2}\frac{\Gamma_Y \mathrm{Br}_X}{m_Y^2}\int d\zeta \frac{\rho_Y(\zeta)}{T_X^2 H(\zeta)} g\left(\frac{T_X}{m_Y}x\right), \tag{9}$$

as illustrated in Fig. 2. The first term of (9) is the primordial Fermi-Dirac distribution of X and the second is the nonthermal repopulation of X, where the ζ integral goes from $T = m_Y/10$ to $t = 10\tau_Y$ that covers the entire period of Y decay.

The secondary component of X has a significantly smaller occupancy, but carries more energy and thereby

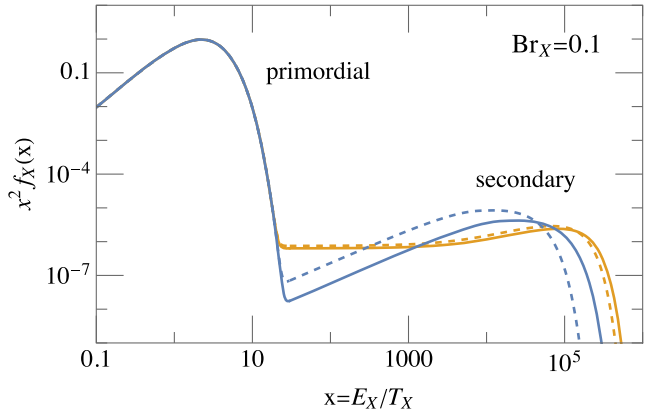

FIG. 2. Phase space distribution of ultrarelativistic X. The blue and orange curves correspond to the two models listed in Table I. Solid (dashed) curve corresponds to $m_X = 10$ keV, $m_Y = 100$ GeV ($m_Y = 1$ PeV), while $\mathrm{Br}_X = 0.1$ for all cases.

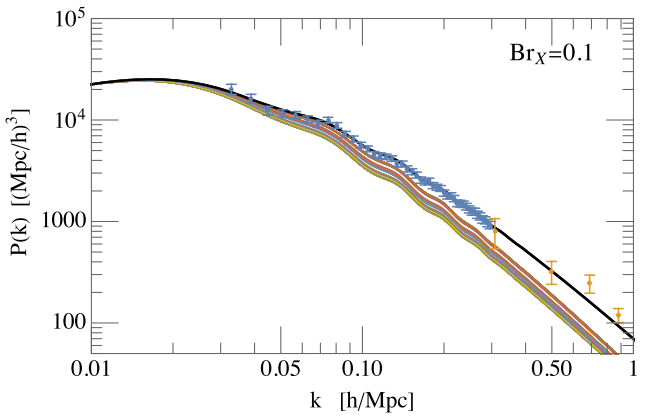

FIG. 3. Primordial matter power spectrum in standard ΛCDM (black solid curve) and diluted DM models listed in Table I (colorful curves). Like Fig. 2, we set $\mathrm{Br}_X = 0.1$. Data points from SDSS DR7 LRG and Lyman-α observations are shown in blue and orange, respectively.

affects structure formations. The shape of the secondary component is roughly independent of m_Y. This follows from Eqs. (2) and (3), where the relic density requires the scaling $m_Y \sim 1/\sqrt{\tau_Y}$ and the reheating temperature is set by the Hubble time $T_{\mathrm{RH}} \sim \sqrt{H} \sim 1/\sqrt{\tau_Y}$. Immediately after $Y \to X$ decay, $E_X \lesssim m_Y$ and $T_X \sim T_{\mathrm{RH}}$. As a result, the kinematic endpoint $x_{\mathrm{max}} \sim m_Y/T_{\mathrm{RH}}$ is held constant for fixed m_X, irrespective of m_Y or τ_Y.

Imprint on the matter power spectrum.—Let us begin with a simple heuristic understanding of how the matter power spectrum is affected, which we then sharpen by a thorough numerical study. The secondary population of X becomes nonrelativistic when the photon temperature drops to

$$T_{\mathrm{NR}} \sim 1\ \mathrm{eV}(n+m) g_*(T_{\mathrm{RH}})^{1/12}, \tag{10}$$

which is rather low for $n + m \sim \mathcal{O}(1)$ and nearly independent of g_*. Above T_{NR}, the DM fluid is made of the nonrelativistic primordial and the relativistic secondary component. The energy density of the latter is more important at temperatures above $T_{\mathrm{NR}}/\mathrm{Br}_X$. In this regime, the effective sound speed of the X fluid is large, which interrupts the regular logarithmic growth of density perturbations in X. This suppresses the primordial matter power spectrum $P(k)$ on length scales smaller than the Hubble radius at temperature $T_{\mathrm{NR}}/\mathrm{Br}_X$, see Fig. 3. The resulting $P(k)$ would thus disagree with the LSS measurements, unless $\mathrm{Br}_X \ll 1$.

We now turn to a quantitative numerical analysis in the parameter space of m_X versus m_Y. For each point we first set the dilutor lifetime τ_Y using Eq. (2). Next, we determine the phase space distribution f_X with Eq. (9) and evolve it with CLASS [27–29] to obtain $P(k)$. We scan over 200 points in the mass range $m_X \in (1\ \mathrm{keV}, 1\ \mathrm{MeV})$ and $m_Y \in (1\ \mathrm{GeV}, 10^{16}\ \mathrm{GeV})$ for both models in Table I. The results are shown by the colored curves in Fig. 3, where we set $\mathrm{Br}_X = 0.1$, while the black solid curve is the fiducial ΛCDM model.

The experimental data points come from the sloan digital sky survey (SDSS) DR7 on luminous red galaxies [30] (blue) and the Lyman-α forest [31] (orange) measurements. All the curves in scenarios with secondary X share a common feature with significant deviations from data in the $k \gtrsim 0.03\ h/\mathrm{Mpc}$ region. These occur at a much lower k compared to other DM production mechanisms such as thermal freeze-in [32,33]. This is mainly due to the large hierarchy between the dilutor and DM mass, required by Eqs. (2) and (3). Based on a simple $\Delta\chi^2$ fit to the data, we find that the LSS data from SDSS sets a much stronger constraint on these scenarios than Lyman-α, making this probe particularly robust. The conflict with data increases with Br_X, which translates into an upper bound in Fig. 4 for the two models in Table I. The result is similar for both cases and the branching ratio of the dilutor decaying into DM is constrained to be

$$\mathrm{Br}_X \lesssim 1\%, \qquad @95\%\mathrm{CL}. \tag{11}$$

This bound is nearly independent of m_Y. It gets slightly relaxed for larger m_Y, because holding the DM relic density fixed in Eq. (2) requires the τ_Y to be shorter, leading to a higher reheating temperature after the decay of the dilutor. The corresponding temperature for the secondary DM component to become nonrelativistic also increases, which is a $\sqrt[12]{g_*}$ effect *à la* Eq. (10). Eventually, this shifts the deviation of $P(k)$ to a slightly higher k and becomes less constraining.

The constraint derived here comes predominantly from the LSS data, which relies only on the evolution of matter density perturbations in the linear regime. LSS thus provides a robust test of these models and we expect similar constraints to apply broadly for models that utilize

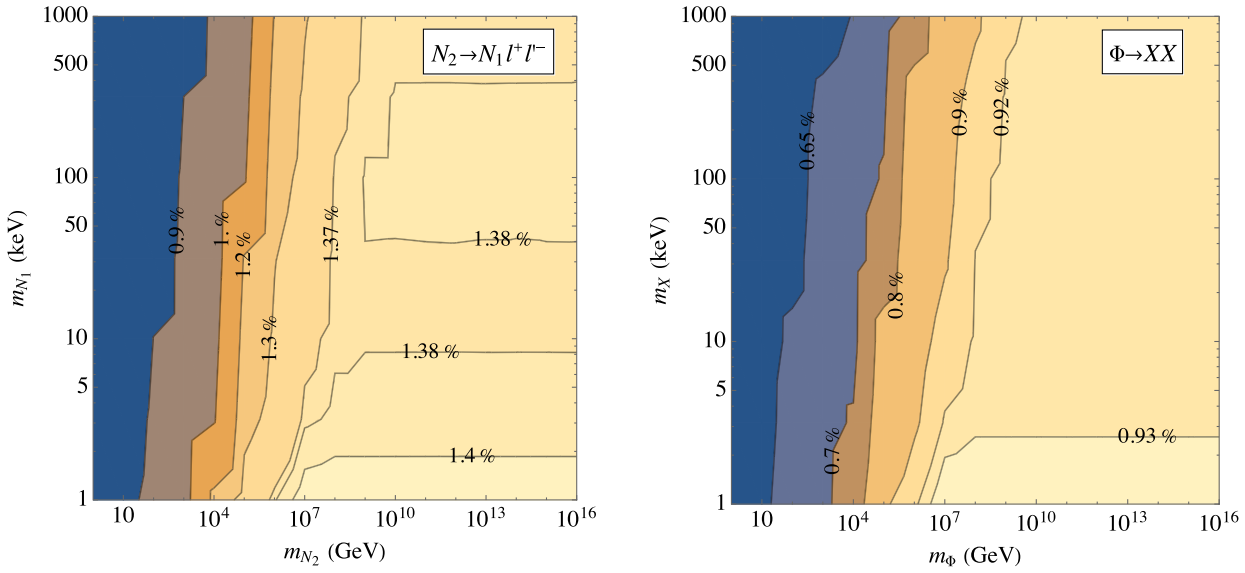

FIG. 4. Upper bound on Br_X, the branching ratio of dilutor Y decaying into X from the fit to LSS data (SDSS DR7 LRG), for the LRSM with $Y = N_2$, $X = N_1$, and a long-lived scalar $Y = \Phi$. For each point in the $m_X - m_Y$ parameter space, the Y lifetime is solved by requiring X to comprise all of the DM in the universe.

the dilution mechanism for addressing the DM relic density.

Our result can be generalized to initial abundances for Y and X beyond the relativistic freeze-out. A subthermal initial population of Y needs to be heavier and/or longer lived in order to provide the same amount of entropy injection. The secondary X particles from Y decay are more energetic and take longer to become matterlike. This impacts the primordial matter power spectrum down to even lower k and leads to a more stringent constraint on Br_X than Eq. (11). On the contrary, starting with a smaller overpopulation of X, the constraint on Br_X will be weaker.

Implications for left-right symmetry.—The LRSM is an elegant framework to accommodate the right-handed neutrino N as DM. Gauging the $SU(2)_L \times SU(2)_R \times U(1)_{B-L}$ necessitates three Ns for anomaly cancellation. The lightest N_1, if cosmologically long-lived, is a DM candidate. Assuming the early universe was sufficiently hot, N_1 would be kept in thermal equilibrium with the known particles by the $SU(2)_R$ gauge interactions and would freeze-out relativistically. Late entropy production is then required to set the relic density of N_1 to the observed DM value.

One (or both) of the heavier right-handed neutrinos, N_2, can play the role of the dilutor [9]. In the simplest scenario, N_2 decays through the exchange of W_R, in close analogy to heavy quarks in the standard model,

$$N_2 \to \ell q \bar{q}', \qquad N_2 \to N_1 \ell \ell', \tag{12}$$

where we assumed that $m_{N_2} > m_\tau$, such that all leptonic channels are open. The first channel plays the desired role of dilution, whereas the second produces energetic N_1 particles that affect the matter power spectrum, as discussed earlier. For N_2 mass well above the electroweak scale, the branching ratio for $N_2 \to N_1 \ell \ell'$ is $1/10$. If the mass of N_2 is below the top quark mass, the ratio grows to $1/7$. Such values are in complete contradiction with the main findings of this work in Eq. (11) and Fig. 4. In this scenario, the entropy dilution mechanism for addressing the DM relic density is thus firmly excluded.

Such a strong constraint can only be evaded with additional non-DM decays of Y. The N_2 could decay via the SM W, mediated either by N_2 and light neutrino ν mixing, or the W-W_R gauge boson mixing. Neutrino mixing comes about if N_2 participates in the type-I seesaw mechanism [34] and is uniquely fixed by $\theta_{N_2\nu} \simeq \sqrt{m_\nu/m_{N_2}}$ [35]. In the presence of the N_2-ν mixing alone, we find that N_2 must be lighter than the W boson for it to be a long-lived dilutor [36]. For the W mediated decay channels to dominate over the W_R mediated ones in order to satisfy the LSS constraint derived in Eq. (11), we need

$$M_{W_R} \gtrsim 55 \text{ TeV} \left(\frac{m_{N_2}}{1 \text{ GeV}}\right)^{1/4}, \tag{13}$$

where we set $m_\nu = \sqrt{\Delta m^2_{\mathrm{at}}} \simeq 0.05$ eV. On the other hand, the W-W_R mixing is of order $\xi_{\mathrm{LR}} \sim M_W^2/M_{W_R}^2$. In this case, N_2 must be heavier than the W boson in order to satisfy the LSS constraint. Producing the correct DM relic density then requires $M_{W_R} > 100$ TeV [36].

It is remarkable that in all cases cosmological measurement can set a much stronger limit on the LRSM than the high-energy colliders [37–39] with the latest limits [40–44] at $M_{W_R} > 5.6$ TeV, and supernova cooling [45]. Another

way of suppressing the repopulation of DM N_1 concerns the flavor structure of the right-handed lepton mixing matrix and the mass spectrum of N_i [10,36].

The $\Delta N_{\rm eff}$ prediction.—The secondary X particles from Y decay contribute to the total energy density of relativistic fluids in the universe until $T_{\rm NR} \sim$ eV. This could lead to a deviation of $\Delta N_{\rm eff}$ from the standard ΛCDM model. At early times, such as the BBN era, the contribution to $\Delta N_{\rm eff}$ can be derived in terms of parameters of the dilution mechanism

$$\Delta N_{\rm eff} \simeq \frac{43}{7}\frac{y\mathrm{Br}_X}{1-y\,\mathrm{Br}_X}\left(\frac{43}{4g_*(T_{\rm RH})}\right)^{1/3}, \tag{14}$$

where the $y\mathrm{Br}_X/(1-y\mathrm{Br}_X)$ factor corresponds to the energy density ratio of the X fluid and the visible sector, immediately after Y decay. Assuming the constraint in Eq. (11) is saturated, we find $\Delta N_{\rm eff} \lesssim 0.062$. This is too small to affect the BBN, but might become relevant for precision cosmological measurements at the future CMB—Stage 4 [46].

On the lower bound for the DM mass.—Let us comment on the limit when $\mathrm{Br}_X \to 0$, i.e., no DM is produced in the dilutor decay. In this case, all DM in the universe is made of the primordial X, which follows a thermal distribution, but has a lower temperature than photons due to entropy production via Y decay. It depends solely on the DM mass,

$$T_X/T_\gamma = 0.16\left(\frac{1\ \mathrm{keV}}{m_X}\right)^{1/3}. \tag{15}$$

Because of the lower temperature ratio compared to alternative production mechanisms, such as the oscillation production for sterile neutrino DM [47–52], the regular warm DM constraints are weaker [8–10,13,16,18]. Lyman-α [53], Milky Way satellite galaxies [54,55], strong lensing observations [56], and the phase space of dwarf galaxies [57–60] set a lower bound on DM mass of several keV.

Outlook.—We explore entropy dilution mechanisms for DM relic density by pointing out and quantifying the signature of dilutor decay to DM on the formation of LSS of the universe. Such a decay mode is common in DM models and the existing cosmological data can set a stringent constraint on its branching ratio. Our result mostly relies on LSS data, which belongs to the linear regime of structure growth and is thus very robust. It can be further improved by future LSS surveys [61,62]. It is also highly complementary to probes of structure formation on small scales and the cosmic microwave background. Our finding offers a new tool for testing and distinguishing particle physics models for diluted DM.

We thank Jeff Dror, Miguel Escudero, and Nicholas Rodd for helpful discussions. M. N. is supported by the Slovenian Research Agency under the research core funding No. P1-0035 and in part by the research Grants No. J1-3013, No. N1-0253, and No. J1-4389. Y. Z. is supported by the Arthur B. McDonald Canadian Astroparticle Physics Research Institute, and the Munich Institute for Astro, -Particle and BioPhysics (MIAPbP), which is funded by the Deutsche Forschungsgemeinschaft (DFG, German Research Foundation) under Germany's Excellence Strategy—EXC-2094–390783311. Y. Z. is grateful to the organizers of the Pollica Summer Workshop supported by the Regione Campania, Università degli Studi di Salerno, Università degli Studi di Napoli "Federico II," i dipartimenti di Fisica "Ettore Pancini" and "E R Caianiello," and Istituto Nazionale di Fisica Nucleare.

*miha.nemevsek@ijs.si
†yzhang@physics.carleton.ca

[1] E. W. Kolb and M. S. Turner, *The Early Universe* (CRC Press, Boca Raton, FL, 1990), Vol. 69.
[2] J. Alexander *et al.*, arXiv:1608.08632.
[3] J. R. Ellis, A. D. Linde, and D. V. Nanopoulos, Phys. Lett. **118B**, 59 (1982).
[4] J. R. Ellis, J. S. Hagelin, D. V. Nanopoulos, K. A. Olive, and M. Srednicki, Nucl. Phys. **B238**, 453 (1984).
[5] R. J. Scherrer and M. S. Turner, Phys. Rev. D **31**, 681 (1985).
[6] T. Moroi and L. Randall, Nucl. Phys. **B570**, 455 (2000).
[7] E. A. Baltz and H. Murayama, J. High Energy Phys. 05 (2003) 067.
[8] T. Asaka, M. Shaposhnikov, and A. Kusenko, Phys. Lett. B **638**, 401 (2006).
[9] F. Bezrukov, H. Hettmansperger, and M. Lindner, Phys. Rev. D **81**, 085032 (2010).
[10] M. Nemevšek, G. Senjanović, and Y. Zhang, J. Cosmol. Astropart. Phys. 07 (2012) 006.
[11] G. Arcadi and P. Ullio, Phys. Rev. D **84**, 043520 (2011).
[12] Y. Zhang, J. Cosmol. Astropart. Phys. 05 (2015) 008.
[13] A. V. Patwardhan, G. M. Fuller, C. T. Kishimoto, and A. Kusenko, Phys. Rev. D **92**, 103509 (2015).
[14] A. Soni, H. Xiao, and Y. Zhang, Phys. Rev. D **96**, 083514 (2017).
[15] R. Contino, A. Mitridate, A. Podo, and M. Redi, J. High Energy Phys. 02 (2019) 187.
[16] J. A. Evans, A. Ghalsasi, S. Gori, M. Tammaro, and J. Zupan, J. High Energy Phys. 02 (2020) 151.
[17] C. Cosme, M. Dutra, T. Ma, Y. Wu, and L. Yang, J. High Energy Phys. 03 (2021) 026.
[18] J. A. Dror, D. Dunsky, L. J. Hall, and K. Harigaya, J. High Energy Phys. 07 (2020) 168.
[19] P. Chanda and J. Unwin, J. Cosmol. Astropart. Phys. 06 (2021) 032.
[20] P. Asadi, T. R. Slatyer, and J. Smirnov, Phys. Rev. D **106**, 015012 (2022).
[21] J. Hasenkamp and J. Kersten, Phys. Rev. D **82**, 115029 (2010).
[22] R. N. Mohapatra and J. C. Pati, Phys. Rev. D **11**, 566 (1975).
[23] G. Senjanović, Nucl. Phys. **B153**, 334 (1979).
[24] R. N. Mohapatra and G. Senjanović, Phys. Rev. Lett. **44**, 912 (1980).
[25] See Supplemental Material at http://link.aps.org/supplemental/10.1103/PhysRevLett.130.121002 provides

a detailed derivation of several key equations presented in the main text, under the sudden decay approximation.
[26] B. S. Acharya, G. Kane, S. Watson, and P. Kumar, Phys. Rev. D **80**, 083529 (2009).
[27] J. Lesgourgues, arXiv:1104.2932.
[28] D. Blas, J. Lesgourgues, and T. Tram, J. Cosmol. Astropart. Phys. 07 (2011) 034.
[29] J. Lesgourgues and T. Tram, J. Cosmol. Astropart. Phys. 09 (2011) 032.
[30] B. A. Reid *et al.*, Mon. Not. R. Astron. Soc. **404**, 60 (2010).
[31] K.-G. Lee *et al.*, Astron. J. **145**, 69 (2013).
[32] F. D'Eramo and A. Lenoci, J. Cosmol. Astropart. Phys. 10 (2021) 045.
[33] Q. Decant, J. Heisig, D. C. Hooper, and L. Lopez-Honorez, J. Cosmol. Astropart. Phys. 03 (2022) 041.
[34] R. N. Mohapatra and G. Senjanović, Phys. Rev. D **23**, 165 (1981).
[35] M. Nemevšek, G. Senjanović, and V. Tello, Phys. Rev. Lett. **110**, 151802 (2013).
[36] M. Nemevšek and Y. Zhang (to be published).
[37] W.-Y. Keung and G. Senjanović, Phys. Rev. Lett. **50**, 1427 (1983).
[38] M. Nemevšek, F. Nesti, G. Senjanović, and Y. Zhang, Phys. Rev. D **83**, 115014 (2011).
[39] M. Nemevšek, F. Nesti, and G. Popara, Phys. Rev. D **97**, 115018 (2018).
[40] V. Khachatryan *et al.* (CMS Collaboration), Phys. Lett. B **770**, 278 (2017).
[41] G. Aad *et al.* (ATLAS Collaboration), Phys. Rev. D **100**, 052013 (2019).
[42] M. Aaboud *et al.* (ATLAS Collaboration), Phys. Lett. B **798**, 134942 (2019).
[43] A. Tumasyan *et al.* (CMS Collaboration), J. High Energy Phys. 04 (2022) 047.
[44] A. M. Abdullahi *et al.*, J. Phys. G **50**, 020501 (2023).
[45] R. Barbieri and R. N. Mohapatra, Phys. Rev. D **39**, 1229 (1989).
[46] K. N. Abazajian *et al.* (CMB-S4 Collaboration), arXiv:1610.02743.
[47] S. Dodelson and L. M. Widrow, Phys. Rev. Lett. **72**, 17 (1994).
[48] A. De Gouvêa, M. Sen, W. Tangarife, and Y. Zhang, Phys. Rev. Lett. **124**, 081802 (2020).
[49] K. J. Kelly, M. Sen, W. Tangarife, and Y. Zhang, Phys. Rev. D **101**, 115031 (2020).
[50] K. J. Kelly, M. Sen, and Y. Zhang, Phys. Rev. Lett. **127**, 041101 (2021).
[51] C. Chichiri, G. B. Gelmini, P. Lu, and V. Takhistov, J. Cosmol. Astropart. Phys. 09 (2022) 036.
[52] C. Benso, W. Rodejohann, M. Sen, and A. U. Ramachandran, Phys. Rev. D **105**, 055016 (2022).
[53] V. Iršič *et al.*, Phys. Rev. D **96**, 023522 (2017).
[54] E. O. Nadler, V. Gluscevic, K. K. Boddy, and R. H. Wechsler, Astrophys. J. Lett. **878**, L32 (2019); **897**, L46(E) (2020).
[55] E. O. Nadler *et al.* (DES Collaboration), Phys. Rev. Lett. **126**, 091101 (2021).
[56] W. Enzi *et al.*, Mon. Not. R. Astron. Soc. **506**, 5848 (2021).
[57] S. Tremaine and J. E. Gunn, Phys. Rev. Lett. **42**, 407 (1979).
[58] A. Boyarsky, O. Ruchayskiy, and D. Iakubovskyi, J. Cosmol. Astropart. Phys. 03 (2009) 005.
[59] V. Domcke and A. Urbano, J. Cosmol. Astropart. Phys. 01 (2015) 002.
[60] C. Di Paolo, F. Nesti, and F. L. Villante, Mon. Not. R. Astron. Soc. **475**, 5385 (2018).
[61] S. Ferraro, N. Sailer, A. Slosar, and M. White, arXiv:2203.07506.
[62] X. Chen, C. Dvorkin, Z. Huang, M. H. Namjoo, and L. Verde, J. Cosmol. Astropart. Phys. 11 (2016) 014.